photonics

MDPI

Article

Statistical Study of Free-Space Optical Transmission Using Multi-Aperture Receivers Under Real-Measured Atmospheric Turbulence

Shutong Liu [1], Shaoqian Tian [1], Baoqun Li [2], Zhi Liu [1,2,*] and Haifeng Yao [3,4]

[1] Institute of Electronic Information Engineering, Changchun University of Science and Technology, Changchun 130022, China; lst@mails.cust.edu.cn (S.L.)
[2] National and Local Joint Engineering Research Center of Space Optoelectronics Technology, Changchun University of Science and Technology, Changchun 130022, China
[3] School of Optoelectronics, Beijing Institute of Technology, Beijing 100081, China
[4] Changsanjiao Research Institute, Beijing Institute of Technology, Jiaxing 314000, China
* Correspondence: liuzhi@cust.edu.cn

Abstract

An experimental investigation was conducted to evaluate the statistical properties and scintillation mitigation performance of multi-aperture free-space optical transmission under real-measured atmospheric turbulence. Continuous monitoring of turbulence parameters over a 24 h period showed that the atmospheric coherence length ranged from 3 to 29 cm, indicating that the experimental link operated predominantly under weak-to-moderate turbulence conditions, while a limited number of measurement intervals exhibited relatively strong scintillation and were included for statistical modelling analysis. An 865 m four-channel receiving link was constructed under the measured turbulence conditions to acquire irradiance data for analysis. The results show that the multi-aperture reception significantly suppresses scintillation, reducing the scintillation index from 0.36 to 0.04 under moderate turbulence. The irradiance probability density functions were fitted using lognormal, Gamma–Gamma, exponentiated Weibull, and Málaga (M) distributions. The M distribution exhibited superior adaptability, with fitting accuracy improved by 18.75% under weak turbulence and 13.16% under moderate turbulence. Further analysis shows that the shape parameters of the M distribution vary systematically with turbulence strength, effectively capturing the turbulence-induced evolution of irradiance statistics and providing experimental support for turbulence channel modelling and the optimisation of FSO diversity reception architectures.

Keywords: multi-aperture reception; scintillation index; light intensity probability density function; Málaga (M) distribution

Check for updates

Received: 16 December 2025
Revised: 5 January 2026
Accepted: 6 January 2026
Published: 8 January 2026

Copyright: © 2026 by the authors. Licensee MDPI, Basel, Switzerland. This article is an open access article distributed under the terms and conditions of the Creative Commons Attribution (CC BY) license.

1. Introduction

Free-Space Optical Communication (FSOC) has been regarded as a significant development direction in future communications technology due to its ultra-high bandwidth, lack of spectrum licencing requirements, and inherent electromagnetic isolation properties [1–3]. However, random perturbations in the refractive index caused by atmospheric turbulence induce random fluctuations in both the intensity and phase of the optical signal at the receiving end, resulting in optical intensity flicker that significantly degrades the performance of the communication link [4,5]. To mitigate the impact of atmospheric turbulence

on FSOC systems, researchers have proposed various techniques for suppressing turbulence, including aperture averaging, adaptive optics, spatial diversity, and Multi-Aperture Reception (MAR) technology. Among these, Multi-Aperture Reception (MAR) employs multiple independent sub-apertures at the receiving end to capture the same optical signal. These signals are then combined in either the optical or electrical domain, thereby smoothing fluctuations caused by atmospheric turbulence, reducing optical intensity flicker at reception, and enhancing signal stability [6].

In recent years, researchers have made significant progress in the design and experimental validation of multi-aperture receiving systems. Martinez et al. proposed an adaptive multi-aperture receiver integrated onto a silicon photonic chip, capable of real-time compensation for flicker caused by turbulence. Its effectiveness was demonstrated in indoor experiments during 10 Gbit/s data transmission [7]. Furthermore, Li et al. designed and experimentally validated an indoor atmospheric turbulence simulation system based on a variable optical attenuator, capable of precisely reproducing specific turbulent channels, thereby facilitating experimental research on FSOC systems [8]. Lao et al. established a 1 km urban-level link employing a four-aperture combination system at the receiving end. They verified that beam combination systems exhibit optimal performance when the sub-aperture spacing exceeds the atmospheric coherence length, with performance degrading as turbulence intensity increases. Pan et al. proposed a multi-aperture adaptive fibre-coupled communication structure and investigated its optical transmission performance, conducting flicker suppression and turbulence compensation experiments based on the Gamma–Gamma turbulent channel model [9]. Recently, Liu Bo et al. experimentally verified near-field long-distance transmitter diversity and aperture averaging, investigating the fit between received data under varying turbulence conditions and different probability density function (PDF) models [10].

Although current research provides significant support for theoretical modelling and systematic experimentation of MAR technology in suppressing turbulence-induced optical intensity flicker, certain shortcomings remain. When modelling the statistical characteristics of FSO signals, common probability density function (PDF) models include the log-normal (LN) distribution, Gamma–Gamma (GG) distribution, exponential-Weibull (EW) distribution, and the Málaga (M) distribution proposed in recent years. These models each possess distinct applicability ranges under varying turbulence intensities. For instance, the LN is suitable for modelling single-path channels under weak turbulence conditions, whereas the GG, owing to its two-parameter nature, can be applied across a wide range of turbulence scenarios from weak to strong [11,12]. The M distribution, owing to its superior fitting capability for signal tail characteristics, demonstrates greater flexibility and accuracy in modelling moderate-to-strong turbulence. Although literature has explored the application of various statistical models in FSO links, experimental data-based modelling and comparative studies of actual light intensity distributions under different turbulence conditions, particularly for multi-aperture receiving systems, remain relatively limited. Furthermore, systematic experimental comparative analyses addressing the differences in fitting accuracy among various models under actual turbulent scenarios remain scarce.

Therefore, this paper established an FSO experimental link based on single-aperture transmission and four-aperture reception. Received optical intensity data for each sub-aperture and the combined signal were collected under varying atmospheric turbulence intensities. Probability density function (PDF) fitting analysis was performed on the experimental data using LN, GG, EW, and M distributions, respectively, to quantitatively evaluate the applicability and fitting accuracy of each model under different turbulence intensities. Experimental results validate the effectiveness of multi-aperture merging

techniques in suppressing signal flicker, whilst revealing the fitting advantages of the M distribution across varying turbulence intensities.

The principal contributions of this paper are as follows:

1. An atmospheric turbulence measurement experiment was established. Utilising an atmospheric coherence length measurement apparatus, continuous 24 h monitoring of atmospheric turbulence conditions during field experiments was conducted, enabling effective extraction of atmospheric coherence length.
2. An 865 m horizontal link was established, employing a four-aperture receiving system at the receiving end. Data acquisition for each sub-aperture at the receiving end utilised combined signals, verifying that multi-aperture reception effectively suppresses optical intensity flicker induced by turbulence.
3. Experimental data from the multi-aperture system were analysed using multiple probability density function (PDF) models. Comparing fitting errors across turbulence intensities revealed that the M distribution demonstrated superior accuracy under all turbulence conditions, effectively characterising the statistical properties of received optical intensity in free-space optical communications.

2. Theoretical Model

2.1. Characteristic Parameters of Atmospheric Turbulence

In multi-aperture receiving systems, two fundamental conditions must typically be satisfied to ensure statistical independence of the receiving channels between sub-apertures. Firstly, the diameter of each sub-aperture should be smaller than the atmospheric coherence length, secondly, the diameter of the sub-apertures should be selected to be less than the atmospheric coherence length to avoid phase distortion and guarantee wavefront coherence within the sub-apertures. It should be noted, however, that in practical outdoor free-space optical communication experiments, this condition serves as a sufficient rather than a strictly necessary requirement [13]. The atmospheric coherence length r_0 (also known as the Fried constant) is a crucial parameter characterising the scale of wavefront coherence induced by atmospheric turbulence. It is typically defined as the diameter of a circle within which the variance of wavefront distortion caused by atmospheric turbulence is 1 rad^2. This represents the aperture diameter at which diffraction-limited performance can be maintained under atmospheric turbulence. The correlation width denotes the spatial scale at which fluctuations in light intensity between two points on the receiving surface exhibit significant correlation. Under weak turbulence conditions, the correlation width is typically determined by the Fresnel zone scale $\sqrt{L/k}$, under moderate turbulence, it approximates the Fried constant, and under strong turbulence, it correlates with the scattering disk size $L/(kr_0)$. Consequently, in practical applications, the correlation width is often approximated as a multiple of the atmospheric coherence length to guide sub-aperture layout design.

According to Kolmogorov's turbulence theory, the atmospheric coherent length can be expressed by the following formula [14]:

$$r_0 = \left[0.423k^2 \int_0^L C_n^2(z)dz\right]^{-3/5} \tag{1}$$

where $k = 2\pi/\lambda$ denotes the light wave beam, λ denotes the light wave wavelength. $C_n^2(z)$ is the atmospheric refractive index structure constant at propagation path, expressed in units of m$^{-2/3}$. L is the path length of light propagation through the atmosphere. When C_n^2 is approximately constant along the path, the above formula may be simplified to

$$r_0 = \left(0.423k^2C_n^2L\right)^{-3/5} \tag{2}$$

It can be observed that, for a fixed wavelength and transmission distance, the stronger the atmospheric turbulence, the shorter the atmospheric coherence length, conversely, when atmospheric turbulence is weaker, the scale at which the light wavefront maintains coherence becomes larger.

The scintillation index is a parameter describing the intensity of atmospheric scintillation, defined as the logarithmic variance of light wave irradiance fluctuations on the receiving plane. It indicates the strength of light intensity fluctuations on the receiving plane [15]. It is expressed as

$$\sigma_I^2 = \frac{\langle I^2 \rangle - \langle I \rangle^2}{\langle I \rangle^2} = \frac{\langle I^2 \rangle}{\langle I \rangle^2} - 1 \tag{3}$$

In the equation, I denotes the received optical intensity, and <·> represents the statistical mean. A higher scintillation index indicates stronger atmospheric scintillation, which in turn exerts a greater impact on optical communication systems [16].

2.2. PDF Model

In free-space laser communication systems, optical intensity scintillation induced by atmospheric turbulence exerts a significant impact on communication performance. The turbulence intensities measured in the field experiments conducted in this study predominantly encompassed weak and moderate turbulence. To comprehensively analyse the statistical characteristics of optical intensity distributions under varying turbulence intensities, this paper introduces the log-normal distribution (LN), Gamma–Gamma distribution (GG), Exponentiated Weibull distribution (EW), and M distribution to fit and compare the experimental data. These models demonstrate good applicability under various turbulence conditions.

The PDF of the log-normal distribution (LN) is expressed as [17].

$$f_{\mathrm{LN}}(I; \sigma_{\ln I}^2) = \frac{1}{I\sqrt{2\pi\sigma_{\ln I}^2}} \exp\left\{ -\frac{\left[\ln(I) + 0.5\sigma_{\ln I}^2\right]^2}{2\sigma_{\ln I}^2} \right\} \tag{4}$$

Here, $\sigma_{\ln I}^2$ denotes the logarithmic variance of irradiance, I represents the normalised irradiance, and $\sigma_{\ln I}^2 = \ln(\sigma_I^2 + 1)$.

The PDF of the Gamma–Gamma distribution (GG) is expressed as [18]

$$f_{GG}(I, \alpha, \beta) = \frac{2(\alpha\beta)^{\frac{\alpha+\beta}{2}}}{\Gamma(\alpha)\Gamma(\beta)} (I)^{\frac{\alpha+\beta}{2}-1} K_{\alpha-\beta}(2\sqrt{\alpha\beta I}) \tag{5}$$

Here, α and β denote shape parameters describing large-scale and small-scale turbulence, respectively, while $K(\cdot)$ represents the Bessel function of the second kind. This model is applicable for modelling under various turbulence intensities, exhibiting particularly favourable fitting performance under moderate turbulence conditions. The flicker index of the GG is expressed as $\sigma_I^2 = \frac{1}{\alpha} + \frac{1}{\beta} + \frac{1}{\alpha\beta}$. Where

$$\alpha = \left\{ \exp\left[\frac{0.49\sigma_R^2}{\left(1 + 1.11\sigma_R^{12/5}\right)^{7/6}} \right] - 1 \right\}^{-1} \tag{6}$$

$$\beta = \left\{ \exp\left[\frac{0.51\sigma_R^2}{\left(1 + 0.69\sigma_R^{12/5}\right)^{5/6}} \right] - 1 \right\}^{-1} \tag{7}$$

The EW exhibits enhanced flexibility in tail control through the introduction of shape adjustment parameters, demonstrating favourable fitting performance when modelled against empirical data. Its probability density function is defined as [19]

$$f_{\mathrm{EW}}(I, \alpha, \beta, \eta) = \frac{\alpha\beta}{\eta}\left(\frac{I}{\eta}\right)^{\beta-1} \exp\left[-\left(\frac{I}{\eta}\right)^{\beta}\right] \times \left\{1 - \exp\left[-\left(\frac{I}{\eta}\right)^{\beta}\right]\right\}^{\alpha-1} \tag{8}$$

In the EW model, the flicker index is related to the shape parameters and, while is a scale parameter associated with the mean irradiance. The flicker index can be expressed as

$$\sigma_I^2 = \frac{\Gamma\left(1 + \frac{2}{\beta}\right) g_2(\alpha, \beta)}{\alpha\left[\Gamma\left(1 + \frac{1}{\beta}\right) g_1(\alpha, \beta)\right]^2} - 1 \tag{9}$$

where $g_n(\alpha, \beta)$ is defined as $g_n(\alpha, \beta) = \sum_{i=0}^{\infty} \frac{(-1)^i \Gamma(\alpha)}{i!(i+1)^{1+n/\beta}\Gamma(\alpha - i)}$, in the formula α, β, and η can be approximated as, $\alpha \simeq \frac{7.220\sigma_I^{2/3}}{\Gamma(2.487\sigma_I^{2/6} - 0.104)}$, $\beta \simeq 1.012(\alpha\sigma_I^2)^{-13/25} + 0.142$, $\eta = \frac{1}{\alpha\Gamma(1+1/\beta)g_1(\alpha,\beta)}$.

The M distribution is a generalised statistical model for light intensity fluctuations. It not only provides a unified description for several commonly used distributions (log-normal, K-distribution, Gamma–Gamma distribution, Rician distribution, etc.), but also possesses strong parametric flexibility, enabling it to adapt to light intensity variations under conditions ranging from weak to strong turbulence. The mathematical expression for the PDF of the M distribution is as follows [20]:

$$P_l(I) = A \sum_{k=1}^{\beta} a_k I^{\frac{\alpha+k}{2}-1} K_{\alpha-k}\left(2\sqrt{\frac{\alpha\beta I}{\gamma\beta + \Omega'}}\right) \tag{10}$$

where, $A = \frac{2\alpha^{\frac{\alpha}{2}}}{\gamma^{1+\frac{\alpha}{2}}\Gamma(\alpha)}\left(\frac{\gamma\beta}{\gamma\beta+\Omega'}\right)^{\beta+\frac{\alpha}{2}}$, $a_k = \binom{\beta-1}{k-1}\frac{1}{(k-1)!}\left(\frac{\Omega'}{\gamma}\right)^{k-1}\left(\frac{\alpha}{\beta}\right)^{\frac{k}{2}}(\gamma\beta + \Omega')^{1-\frac{k}{2}}$, $\Omega' = \Omega + 2\rho b_0 + 2\sqrt{2b_0\Omega\rho}\cos(\varphi_A - \varphi_B)$, where α is a positive real number related to the effective number of large-scale vortices during scattering, β is a natural number representing the number of attenuation events, $K_{\mathrm{v}}()$ is the Bessel function of the second kind, Ω' denotes the average optical power, φ_A and φ_B and, respectively, represent the phase of the line-of-sight propagation component and the coupled component of the optical wave in the turbulent atmospheric channel [21,22].

3. Experimental System Setup

To achieve a more precise analysis of turbulence intensity within the experimental environment, measurements of the atmospheric coherence length along the experimental link were first conducted, followed by a four-aperture free-space optical reception experiment.

3.1. Experimental Measurement of Atmospheric Turbulence Parameters

Using the atmospheric coherent length measurement apparatus constructed in the laboratory, variations in atmospheric turbulence characteristic parameters r_0 along the experimental path were measured. The K-means clustering algorithm proposed in refer-

ence [23] was employed to achieve effective extraction of r_0. This experiment commenced at 08:00 on 20 May 2025 and concluded at 08:00 on 21 May 2025, continuously monitoring atmospheric turbulence variations over a 24 h period.

Figure 1 illustrates the measured atmospheric coherence length as a function of time. The graph demonstrates significant fluctuations in atmospheric coherence length throughout the diurnal cycle, with variations ranging from approximately 3 cm to 29 cm. The atmospheric coherence length of plane waves can be inverted from r_0 to obtain C_n^2 via formula $r_0 = \left(0.423k^2C_n^2L\right)^{-3/5}$, yielding a 24 h variation curve for C_n^2. As can be seen from Figure 2, the 24 h C_n^2 variation range is between 10^{-15} and 10^{-13}, with atmospheric turbulence fluctuating between weak and moderately strong turbulence. From 08:00 to 16:00, turbulence remained at a moderately strong level. Particularly between 09:00 and 12:00, the atmospheric refractive index structure constant C_n^2 fluctuated between $2.021 \times 10^{-14}\mathrm{m}^{-2/3} \sim 1.138 \times 10^{-13}\mathrm{m}^{-2/3}$, corresponding to an atmospheric coherence length r_0 ranging from 1.990 cm to 5.613 cm. During this period, the mean value of C_n^2 was $4.026 \times 10^{-14}\mathrm{m}^{-2/3}$, with the corresponding r_0 being 3.848 cm, Between 18:00 and 05:00, the atmosphere exhibited weak turbulence, particularly between 23:00 and 04:20 when turbulence levels ranged from $2.952 \times 10^{-15}\mathrm{m}^{-2/3} \sim 6.937 \times 10^{-15}\mathrm{m}^{-2/3}$. The atmospheric coherence length r_0 varied between 10.663 cm and 17.805 cm during this period, with C_n^2 averaging 5.097×10^{-15} $\mathrm{m}^{-2/3}$ and r_0 averaging 13.081 cm. The medium-to-strong turbulence experiments for the multi-aperture reception tests commenced in the morning, while the weak turbulence experiments were scheduled to begin after midnight.

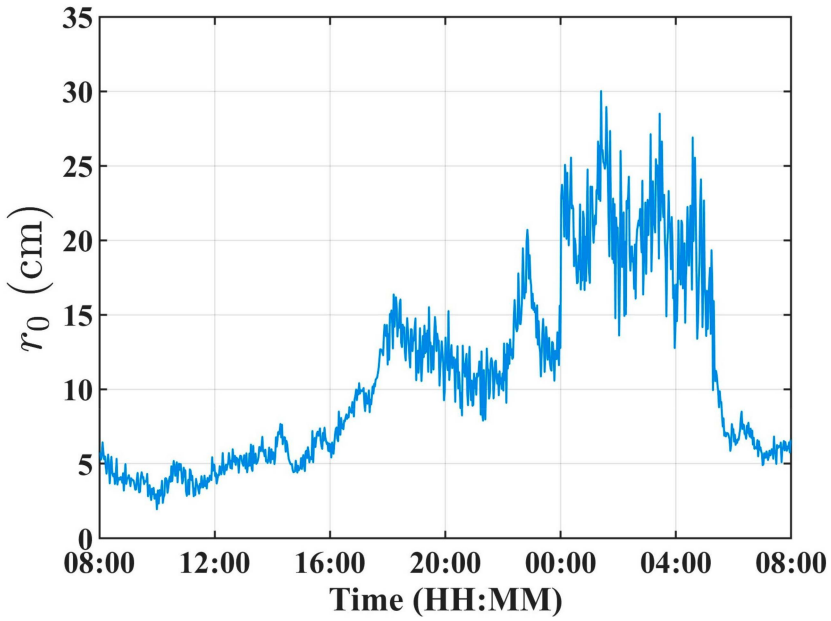


Figure 1. This is 24 h variation in atmospheric coherence length r_0.

To provide a clear classification of turbulence regimes, the scintillation index (SI) is adopted as the primary classification metric in this work. The turbulence conditions are classified as weak turbulence for $\sigma_I^2 < 0.3$, moderate turbulence for $0.3 \leq \sigma_I^2 \leq 1$, and relatively strong turbulence for $\sigma_I^2 > 1$. According to this criterion, the majority of the 24 h experimental data correspond to weak-to-moderate turbulence conditions.

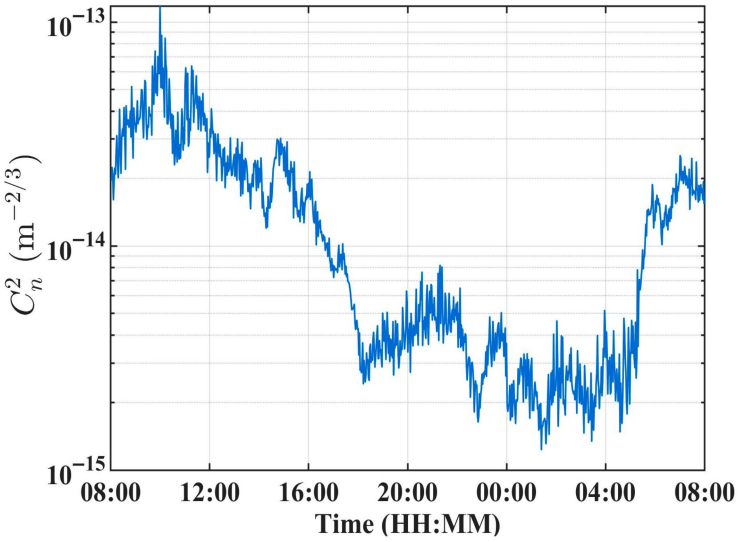


Figure 2. This is the 24 h variation in the atmospheric refractive index structure constant.

3.2. Experiment on Free-Space Optical Transmission Using Four Aperture Receivers

To validate the statistical characteristics of light intensity reception across sub-apertures within a multi-aperture receiving system, an 865 m urban free-space laser communication link was established. The experiment was conducted in Changchun City, Jilin Province, China, under environmental conditions where the temperature fluctuated between 18 °C and 22 °C, the Air Quality Index (AQI) ranged from 30 to 39, relative humidity varied between 60% and 77%, wind speed was 1 to 2 m/s, visibility spanned 14–16 km, and atmospheric pressure was approximately 1005 hPa. The experimental setup is illustrated in Figure 3. The transmitter was positioned on the 13th floor of the Science and Technology Building in the South Campus of Changchun University of Science and Technology, while the receiver was situated on the 9th floor of the Second Teaching Building in the East Campus. For analytical convenience, the receiving system employed a four-aperture configuration with equidistant spacing, arranged in a regular square array. Given the sufficiently small focal length of the receiving collimator, no correction for arrival angle fluctuations was applied in this experiment.

To ensure the independence of each sub-channel, the experimental correlation width was set at 3.66 cm, with the atmospheric coherence length remaining below 35 cm throughout the experimental period. Consequently, the sub-aperture spacing was established at 37 cm, whilst the sub-aperture diameter was ultimately determined to be 50 mm to satisfy the sub-channel independence requirement. The sub-aperture diameter remained fixed at 50 mm throughout the experiment, representing a practical compromise between optical collection efficiency, alignment error, and long-term outdoor stability.

The optical signal power received by each sub-aperture was measured using photodetector (model KG-PR-200M-A-FC, Beijing Kangguan Century Optoelectronics Technology Co., Ltd., Beijing, China) was used to convert the received optical signal into an electrical signal. Synchronous acquisition and recording of the received power were performed via a 24-bit, four-channel isolated data acquisition card, the VK701H+ v2. In the present experimental system, the received optical signals from different sub-apertures are combined using an optical beam combiner located at the backend of the sub-aperture array. Each sub-aperture independently collects the incident optical field, and the corresponding optical beams are subsequently guided to the beam combiner, where they are superimposed to form a single combined optical signal. The combining process is performed in the optical domain and is inherently incoherent, the resulting combined signal corresponds to the

direct superposition of the optical intensities contributed by each sub-aperture, which is equivalent to an equal-gain combining scheme. As a result, the combined irradiance can be expressed as the summation of the individual sub-aperture irradiances. The experimental link's receiving and transmitting end configurations are illustrated in Figure 3. A large-aperture telescope was employed at the transmitting end, while the receiving end utilised the outer ring of the apparatus's four apertures to receive the optical signals.

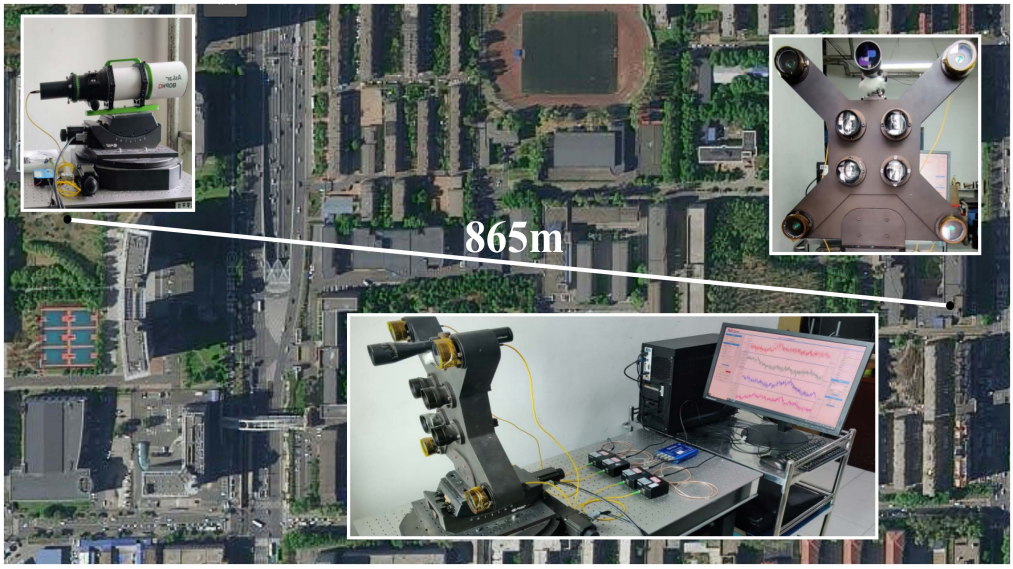


Figure 3. Schematic Diagram of the 865 m Experimental FSO Link.

To analyse the statistical characteristics of received light intensity across sub-apertures under varying turbulence intensities and their fit to probability density function models, experiments were conducted during two representative time periods: morning and early morning, corresponding to moderate and weak turbulence conditions, respectively. Each sampling session lasted one minute at a sampling frequency of 1 MHz, with the entire experimental process completed within ten minutes. According to frozen turbulence theory, atmospheric turbulence conditions may be considered stable within this timescale. Specific system parameters are detailed in Table 1.

Table 1. Parameters of the Multi-aperture Receiver Experimental System.

Experimental Parameters	Parameter Value
wavelength	1550 nm
transmission distance	865 m
transmission power	24 dBm
divergence angle	0.5 mrad
number of receiving apertures	4
sub-aperture spacing	37 cm
sampling rate	1 MHz
receiving aperture dimensions	50 mm

Experimental results for two typical atmospheric turbulence intensities are shown in Figures 4 and 5. It can be observed that the light intensity and relative variance received by the four sub-apertures are comparable. At a correlation width of 2.75 cm, the relative variance of light intensity fluctuations decreases from 0.36 to 0.04. At a correlation width of 17.35 cm, the relative variance of light intensity fluctuations remains essentially unchanged.

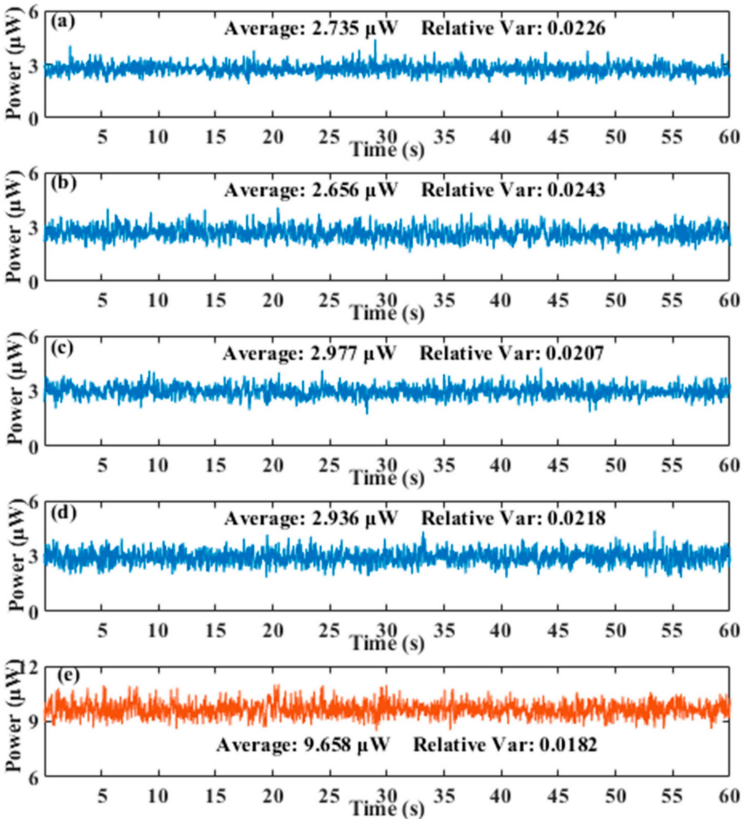


Figure 4. At a relevant width ρc = 17.35 cm (21 May 2025 02:20), the light intensities of the four input beams (**a**–**d**) and the combined output beam (**e**).

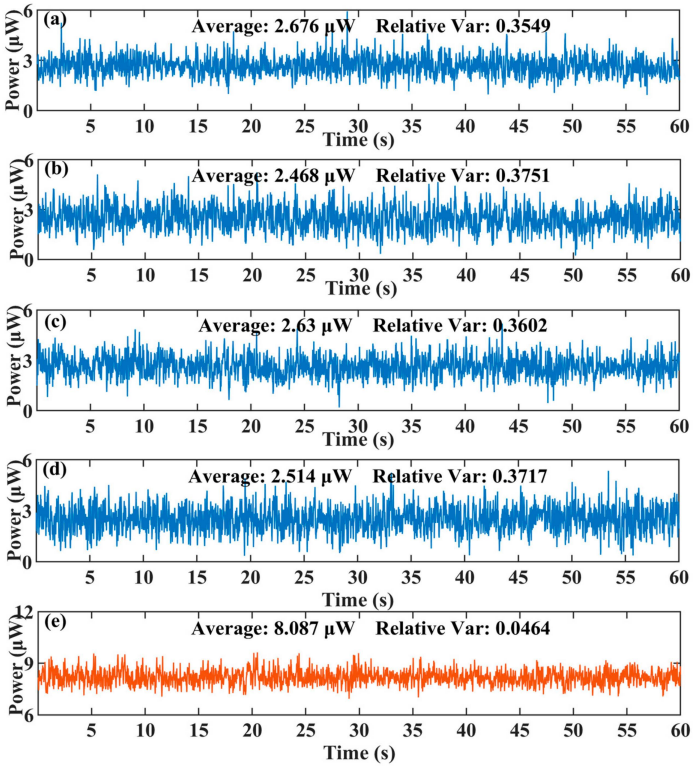


Figure 5. At a relevant width ρc = 2.75 cm (20 May 2025 09:50), the light intensities of the four input beams (**a**–**d**) and the combined output beam (**e**).

4. Results and Discussion

4.1. Statistical Fitting of Sub-Aperture Irradiance Under Different Turbulence Conditions

To quantitatively evaluate the fitting performance of different statistical models under varying turbulence intensities, this study modelled the probability distribution of received power across various aperture sizes under both weak and moderately strong turbulence conditions. LN, EW, Gamma–Gamma, and M distributions were employed for fitting. The results were then compared with measured data to evaluate each model's applicability and fitting accuracy across different turbulence scenarios.

To investigate the channel characteristics of each sub-aperture, the Levenberg–Marquardt least-squares fitting algorithm, implemented using the lsqcurvefit function in MATLAB R2023a, was employed to fit both experimental data and theoretical PDFs [24]. Here, the PDF model first fits the data in the linear domain before displaying the results in the logarithmic domain. It should be noted that parameter estimation for each model is performed entirely in the linear domain, whereas the logarithmic coordinate system is adopted only for visualisation purposes, in order to more clearly illustrate the variation characteristics of the probability density function in low-irradiance regions dominated by deep fading events. As a result, deviations between fitted models and experimental histograms at higher irradiance levels may appear more pronounced in logarithmic plots, particularly where the number of high-irradiance samples is limited due to the long-tailed nature of turbulence-induced irradiance fluctuations.

Figures 6 and 7 display the fits of the sub-aperture experiment's received optical intensity to the LN, GG, EW, and M distribution models under weak turbulence and moderate-to-strong turbulence conditions, respectively. The results indicate that under weak turbulence, the distribution shapes of the received signals from each sub-aperture are approximately symmetric with rapid tail decay. The M-distribution and LN-distribution exhibit the smallest root mean square error (RMSE), demonstrating their greater accuracy in characterising the statistical properties under weak turbulence conditions. As atmospheric turbulence intensified, signal fluctuations increased, distributions deviated from Gaussian shapes, tails elongated, exhibiting typical turbulent speckle characteristics. At this stage, traditional LN and GG models fail to adequately fit the tails. The M-distribution, however, incorporates additional shape parameters (such as α and β), enabling more flexible characterisation of asymmetric and long-tailed distributions, with significantly lower fitting errors than other models. Particularly in combined signal statistics, the M-distribution demonstrates robustness and generalisability for signals averaged across multiple apertures.

4.2. Statistical Modelling of Combined-Aperture Irradiance

Under weak turbulence and moderate turbulence conditions, the combined experimental received light intensity was fitted to various PDFs. Figure 8 shows that under weak turbulence, the M-distribution exhibits a fitting error of 0.039, demonstrating superior fitting performance compared to the EW (0.048) and Gamma–Gamma distribution (0.061), representing an 18.75% improvement over the next-best model. Under medium turbulence, the M-distribution exhibits a fitting error of 0.033, demonstrating superior fitting performance compared to the EW (0.038) and Gamma–Gamma distribution (0.052), with an improvement of 13.16% over the next-best model. The results indicate that, when employing optimal fitting parameters, the M distribution is suitable for statistical modelling and performance analysis of multi-aperture receiving systems under varying turbulence intensity conditions.

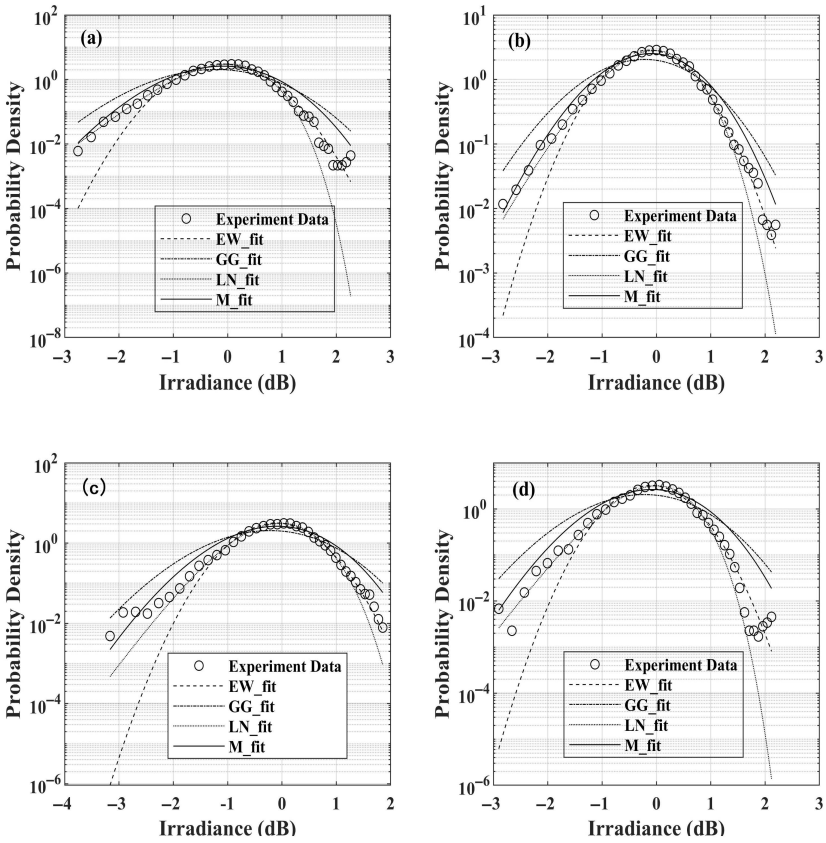


Figure 6. Atmospheric Coherence Length r_0 **= 27.1** cm Sub-aperture and Different PDF Fitting, (**a**–**d**) represent four distinct sub-apertures, respectively.

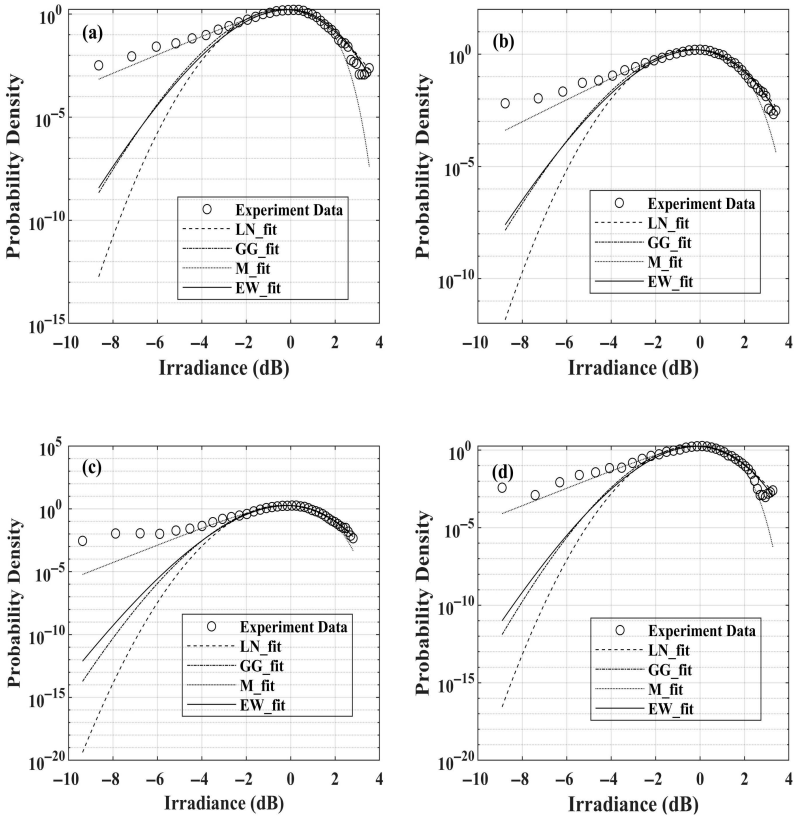


Figure 7. Atmospheric Coherence Length r_0 **= 5.4** cm Sub-aperture and Different PDF Fitting, (**a**–**d**) represent four distinct sub-apertures, respectively.

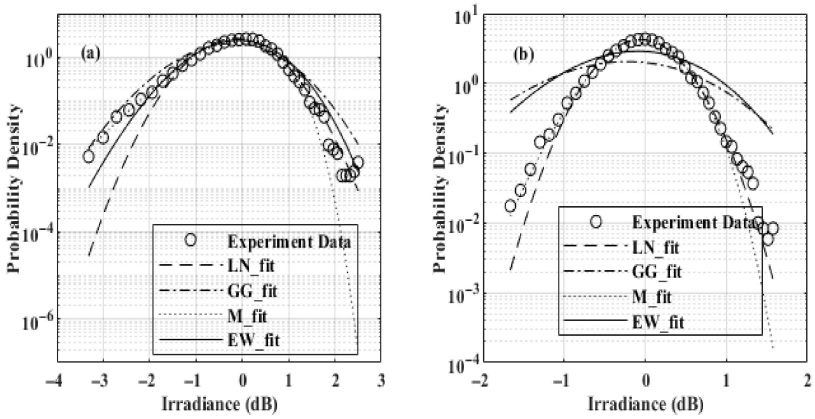


Figure 8. (**a**) Under atmospheric coherence length r_0 **= 27.1** cm conditions, the combined received signal fitted with different PDFs. (**b**) Under atmospheric coherence length r_0 **= 5.4** cm conditions, the combined received signal fitted with different PDFs.

It can be observed in Figure 8 that the Málaga (M) distribution provides excellent agreement with the experimental data in the low-irradiance region, which is primarily influenced by deep fading and scintillation effects. At higher irradiance levels, slight discrepancies become more visible in the logarithmic representation, mainly due to the reduced number of high-irradiance samples and finite-sample statistical effects, rather than a fundamental limitation of the statistical model.

4.3. Experimental Evolution of Málaga Distribution Parameters with Turbulence Strength

Table 2 lists the optimal fitting parameters for each statistical model used to generate the probability density function curves in Figures 6 and 7 under different turbulence conditions. Additionally, the table includes the actual scintillation index (SI) calculated from experimental data, alongside theoretical SI values derived from the fitting parameters of each PDF model. These serve to comparatively evaluate the fitting accuracy of the respective models. It should be noted that Table 2 contains data points where the atmospheric coherence length is close to or slightly below the sub-aperture diameter. These correspond to measurement regions with relatively strong turbulence over short time periods and have been incorporated to extend the scope of the statistical modelling.

Figure 9 presents experimental results showing the variation of M-distribution parameters α, β, ρ, and Ω with the flicker index. It is evident that different parameters exhibit distinct responses to turbulence intensity. Specifically, the shape parameters α and β decrease monotonically with the flicker index, exhibiting a significant reduction in magnitude. As the scintillation index increases from 0.02 to 3.65, α decreases from 20 to 1 and β from 18 to 1. This trend aligns with their physical interpretations: since α relates to large-scale scattering and β describes small-scale attenuation, both scattering structures are weakened when turbulent perturbations intensify and reduce light field coherence, consequently leading to a marked reduction in both α and β as the flicker index increases. Furthermore, the variations in α and β are well-fitted by the logistic function, indicating a stable mapping relationship between them across different turbulence intensities. This establishes the M distribution as the key parameter most effectively reflecting turbulence strength.

In contrast, the relationship between ρ and Ω with respect to SI does not exhibit a monotonic trend. Experimental results indicate that ρ experiences a brief increase in the moderate turbulence range, while approaching zero under both weak and strong turbulence conditions. Ω, meanwhile, declines rapidly when SI < 1 before subsequently tending towards zero. This outcome reflects the fact that these two parameters are primarily determined by the physical characteristics inherent to the system structure itself. ρ represents

the coefficient coupling scattered power to the optical axis component, while Ω denotes the line-of-sight (LOS) field average power. These parameters are predominantly governed by beam directivity, energy dissipation, and system geometry, rather than being solely driven by turbulence intensity. Consequently, their lack of a unified trend with respect to SI is physically well-founded.

Table 2. Optimal fitting parameters and flicker indices for PDF generation under different turbulence conditions.

r_0	Conditions	LN	GG		EW				
(cm)	$\sigma^2_{I_{data}}$	σ^2_{lnI}	α_{fit}	β_{fit}	$\sigma^2_{I_{GG}}$	α	β	η	$\sigma^2_{I_{EW}}$
28.9	0.02	0.02	50	50	0.05	3.65	2.81	0.84	0.03
27.1	0.15	0.15	8.7	75.5	0.18	4.23	1.53	0.72	0.18
24.8	0.37	0.37	6.2	55.1	0.37	4.62	1.37	0.68	0.37
19.6	0.71	0.62	3.6	3.6	0.71	5.48	1.02	0.25	0.71
13.7	1.24	0.79	3.0	3.0	1.30	5.69	0.54	0.19	1.24
8.2	1.33	0.92	2.5	2.5	1.24	6.24	0.37	0.13	1.33
5.4	2.48	2.08	1.8	1.8	2.48	5.81	0.29	0.07	2.35
3.3	3.65	2.48	1.2	1.2	3.65	5.47	0.21	0.03	3.42
r_0	Conditions	M distribution							
(cm)	$\sigma^2_{I_{data}}$	α	β	ρ	Ω	$\sigma^2_{I_M}$			
28.9	0.02	20	16	0	1	0.03			
27.1	0.15	17	14	0	1	0.16			
24.8	0.37	11	10	1	0.5	0.37			
19.6	0.71	6	7	1	0.5	0.71			
13.7	1.24	6	4	1	0.5	1.24			
8.2	1.33	4	2	0	1	1.33			
5.4	2.48	2	1	0	1	2.45			
3.3	3.65	1	1	0	1	3.52			

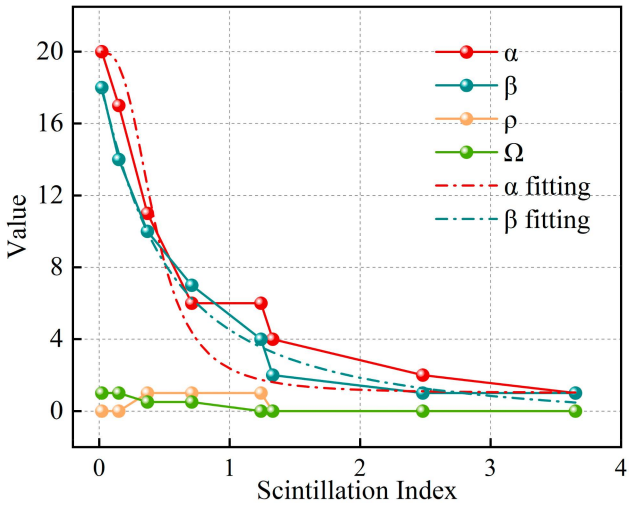


Figure 9. M distribution parameters as a function of the flicker index.

In summary, α and β exhibit high sensitivity to turbulence intensity, with their variations under SI reflecting turbulence's direct influence on light intensity statistics. In contrast, ρ and Ω are more constrained by the system's energy distribution and structural characteristics, being less affected by turbulence fluctuations. This study, based on field experimental data, reveals the differential responses of various parameters within the M-distribution to turbulence, providing new physical rationale for establishing turbulence statistical models grounded in the M-distribution.

5. Conclusions

To investigate the performance of multi-aperture receiving systems in free-space laser communications, this paper first obtained atmospheric turbulence intensity parameters through field measurements, effectively extracting the 24 h atmospheric coherence length. Subsequently, an outdoor experimental platform featuring a four-aperture receiving system was established based on an 865 m free-space link. Experiments demonstrated that the multi-aperture receiving structure effectively suppresses light intensity flicker fluctuations caused by turbulence. Building upon this foundation, four representative statistical models—the LN model, Gamma–Gamma model, EW distribution, and Generalised M distribution—were employed to perform PDF fitting on received optical intensity data under varying turbulence conditions, yielding optimal fitting parameters. Results demonstrate that the Generalised M distribution exhibits superior modelling capability under both weak and moderate turbulence conditions. Compared to traditional PDF models, it provides more stable fitting performance in multi-aperture systems, thereby establishing a theoretical basis for subsequent system performance modelling and optimisation. It is important to emphasise that flicker suppression in multi-aperture receiving systems is primarily governed by spatial diversity conditions, and thus the sub-aperture spacing must be substantially greater than the turbulence-induced correlation width. This condition remained consistently satisfied throughout the entire experimental process. Even when condition D was not strictly met, diversity gain was still predominantly driven by this factor.

Author Contributions: Conceptualization, S.L. and Z.L.; methodology, S.L.; software, S.L.; validation, S.L., S.T. and Z.L.; formal analysis, S.L. and B.L.; investigation, B.L.; resources, S.T.; data curation, S.L.; writing—original draft preparation, S.L.; writing—review and editing, S.L. and S.T.; visualisation, S.L.; supervision, H.Y.; project administration, Z.L.; funding acquisition, Z.L. All authors have read and agreed to the published version of the manuscript.

Funding: This research was funded by National Natural Science Foundation of China Ye Qisun Science Foundation grant number U2141231.

Institutional Review Board Statement: Not applicable.

Informed Consent Statement: Informed consent was obtained from all subjects involved in the study.

Data Availability Statement: No data was used for the research described in the article. Data are contained within the article.

Conflicts of Interest: The authors declare no conflicts of interest.

References

1. Jeon, H.B.; Kim, S.M.; Moon, H.J.; Kwon, D.H.; Lee, J.W.; Chung, J.M.; Han, S.K.; Chae, C.B.; Alouini, M.S. Free-space optical communications for 6G wireless networks: Challenges, opportunities, and prototype validation. *IEEE Commun. Mag.* **2023**, *61*, 116–121. [CrossRef]
2. Bagga, S.; Madhu, C.; Thangjam, S. A precise review on different aspects of free space optical communication (FSOC) systems. *Wirel. Pers. Commun.* **2024**, *137*, 1641–1661. [CrossRef]
3. Li, D.; Yan, B.; Yuan, Y.; Cai, Y.; Hao, Z.; Li, J. Real-time demonstration of multi-gigabit/s free-space optical communications employing femtosecond laser filaments in complex environment. *J. Light. Technol.* **2024**, *42*, 4402–4409. [CrossRef]
4. Li, J.; Yao, H.; Wang, J.; Cao, Z.; Wang, W.; Dong, K.; Hao, Q.; Song, Y.; Liu, X.; Liu, Z.; et al. Experimental demonstration of a free space optical wireless video transmission system based on image compression sensing algorithm. *Opt. Express* **2023**, *31*, 41479–41495. [CrossRef] [PubMed]
5. Agarwal, H.; Mishra, D.; Kumar, A. A deep-learning approach for turbulence correction in free space optical communication with Laguerre–Gaussian modes. *Opt. Commun.* **2024**, *556*, 130249. [CrossRef]

6. Vorontsov, M.; Filimonov, G.; Ovchinnikov, V.; Polnau, E.; Lachinova, S.; Weyrauch, T.; Mangano, J. Comparative efficiency analysis of fiber-array and conventional beam director systems in volume turbulence. *Appl. Opt.* **2016**, *55*, 4170–4185. [CrossRef] [PubMed]
7. Martinez, A.I.; Cavicchioli, G.; Seyedinnavadeh, S.; Zanetto, F.; Sampietro, M.; D'Acierno, A.; Morichetti, F.; Melloni, A. Self-adaptive integrated photonic receiver for turbulence compensation in free space optical links. *Sci. Rep.* **2024**, *14*, 20178. [CrossRef] [PubMed]
8. Li, L.; Ji, N.; Wu, Z.; Wu, J. Design and experimental demonstration of an atmospheric turbulence simulation system for free-space optical communication. *Photonics* **2024**, *11*, 334. [CrossRef]
9. Pan, Z.; Li, Y.; Shen, Y.; Li, Z.; Huang, G.; Geng, C.; Li, X. Multi-aperture adaptive fiber-coupled free-space optical communication system: Scintillation mitigation and turbulence compensation experiment based on Gamma-Gamma channel modeling. *IEEE Photonics J.* **2025**, *in press*. [CrossRef]
10. Guo, M.; Lu, Z.; Wang, Y.; Li, B.; Xu, D.; Duan, S.; Yao, Y.; Zhang, H.; Lin, W.; Liu, H.; et al. Experimental investigation of transmission diversity and reception aperture averaging for terrestrial near-field long-distance free-space optical turbulence residence. *Opt. Laser Technol.* **2025**, *188*, 112979. [CrossRef]
11. Wang, Z.; Zhong, W.D.; Fu, S.; Lin, C. Performance comparison of different modulation formats over free-space optical (FSO) turbulence links with space diversity reception technique. *IEEE Photonics J.* **2009**, *1*, 277–285. [CrossRef]
12. Bhatnagar, M.R.; Ghassemlooy, Z. Performance analysis of gamma–gamma fading FSOMIMOlinks with pointing errors. *J. Light. Technol.* **2016**, *34*, 2158–2169. [CrossRef]
13. Andrews, L.C.; Beason, M.K. *Laser Beam Propagation in Random Media: New and Advanced Topics*; SPIE Press: Bellingham, WA, USA, 2023; pp. 17–55.
14. Sha, Y.; Jing, X.; Wu, Y.; Hou, Z.H. Influence of Signal-to-Noise Ratio on Atmospheric Coherence Length Measured by DIMM. *J. Atmos. Environ. Opt.* **2018**, *13*, 178.
15. Guha, S.; Gonzalez, L.P. *Laser Beam Propagation in Nonlinear Optical Media*; CRC Press: Boca Raton, FL, USA, 2014; Volume 1.
16. Cox, M.A.; Mphuthi, N.; Nape, I.; Mashaba, N.; Cheng, L.; Forbes, A. Structured light in turbulence. *IEEE J. Sel. Top. Quantum Electron.* **2020**, *27*, 1–21. [CrossRef]
17. Al-Habash, M.A.; Andrews, L.C.; Phillips, R.L. Mathematical model for the irradiance probability density function of a laser beam propagating through turbulent media. *Opt. Eng.* **2001**, *40*, 1554–1562. [CrossRef]
18. Luo, Y.; Dang, A. Finite-state Markov modeling of Gamma–Gamma fading FSO links with pointing errors. *Opt. Laser Technol.* **2024**, *172*, 110528. [CrossRef]
19. Panić, S. Statistical modelling of atmospheric turbulence in free-space optical communication systems. In Proceedings of the Sinteza 2024—International Scientific Conference on Information Technology, Computer Science, and Data Science, Singidunum University, Belgrade, Serbia, 16 May 2024; pp. 184–190.
20. Chen, D.; Tang, L.; Wang, M.; Liu, Y. Performance analysis of MIMO FSO adaptive mode switching in Málaga turbulent channels with pointing error. *Opt. Laser Technol.* **2025**, *181*, 111967. [CrossRef]
21. Ansari, I.S.; Yilmaz, F.; Alouini, M.S. Performance analysis of free-space optical links over Málaga ($\mathcal{M}$) turbulence channels with pointing errors. *IEEE Trans. Wirel. Commun.* **2015**, *15*, 91–102. [CrossRef]
22. Jurado-Navas, A.; Garrido-Balsells, J.M.; Paris, J.F.; Puerta-Notario, A.; Awrejcewicz, J. A unifying statistical model for atmospheric optical scintillation. In *Numerical Simulations of Physical and Engineering Processes*; InTech: Rijeka, Croatia, 2011; pp. 181–205.
23. Yu, J.; Yao, H.; Liu, Z.; Wang, W.; Tian, S.; Cao, Z.; Dong, K.; Gao, S.; Bai, F. Method for extracting turbulence characteristic parameters for six-aperture structures. *Infrared Laser Eng.* **2024**, *53*, 20240322.
24. Nistazakis, H.E.; Karagianni, E.A.; Tsigopoulos, A.D.; Fafalios, M.E.; Tombras, G.S. Average capacity of optical wireless communication systems over atmospheric turbulence channels. *J. Light. Technol.* **2009**, *27*, 974–979. [CrossRef]

Disclaimer/Publisher's Note: The statements, opinions and data contained in all publications are solely those of the individual author(s) and contributor(s) and not of MDPI and/or the editor(s). MDPI and/or the editor(s) disclaim responsibility for any injury to people or property resulting from any ideas, methods, instructions or products referred to in the content.